**Proceedings of the ASME 2015 International Design Engineering Technical Conferences & Computers and Information in Engineering Conference**
**IDETC/CIE 2015**
**August 2-5, 2015, Boston, USA**

**DETC2015-47330**



# DRAFT: ANALYSIS AND DESIGN OF A TWO DEGREE OF FREEDOM HOECKENS-PANTOGRAPH LEG MECHANISM

**Dmitri Fedorov***
École Polytechnique de Montréal
Montréal, Québec, H3C 3A7
Canada
dmitri.fedorov@polymtl.ca

**Lionel Birglen**
École Polytechnique de Montréal
Montréal, Québec, H3C 3A7
Canada
lionel.birglen@polymtl.ca

## ABSTRACT

*Hoeckens and Chebychev linkages have been widely discussed in the literature as design solutions to build single degree of freedom (DOF) leg mechanisms. Compared to fully actuated legs, often bio-inspired, they offer an unmatched simplicity. However, due to their limited motion capability, they can only be used when the traversed terrain is of limited difficulty. In order to alleviate this drawback, a novel design with a second DOF is proposed in this paper. The introduced mechanism is composed of a Hoeckens linkage augmented by a Pantograph for which the position of the pivot can be changed through an additional rotating link. Screw theory is used to determine the kinematic equations of the mechanism, its singular configurations, and its attainable workspace. Subsequently, an optimization of the geometric parameters is performed to maximize performance indices pertaining to the size of the mechanism's workspace. Finally, possible use of compliant joints is discussed.*

## INTRODUCTION

Although the simplicity, effectiveness and reliability of the wheel make it an obvious choice for most mobile machine applications, it does not offer the same obstacle-avoidance capabilities as walking, which is the main locomotion mode of most terrestrial animals. While a substantial research effort is being invested towards designing complex serial robotic solutions mimicking human or animal legs, alternative mechanical designs using as few as a single degree of freedom to control the leg endpoint trajectory are still being developed. However, this reduced complexity comes at the price of having a fixed gait [1]. In the present paper, the addition of a second DOF to a one-DOF robotic leg is proposed and analyzed. This addition is intended to enable gait adaptation during the leg operation.

Generally, a suitable leg trajectory (when unspecified, a particular endpoint of the foot of the leg is considered) forms an approximatively straight line with respect to the body during the supporting phase, and a more arbitrary curve when the leg is raised and brought back during the swinging phase. Various planar 4-link and 6-link mechanisms have been studied for such an application [2]. The generated trajectory can subsequently be amplified by means of a second mechanism to increase motion range. Compact solutions where amplification is attained by means of an embedded pantograph have been proposed in the literature [3, 4]. One of the most common trajectory generators is the Hoeckens linkage, also referred to as Chebychev's Lambda mechanism.

Designs where the path is amplified by a Hart linkage [5] or various pantograph linkages [6–8] have recently been proposed. In particular, four techniques to increase step height on demand using a prismatic actuator have been proposed for the Hoeckens-pantograph mechanism in [9]. The proposed mechanism (cf. Fig. 1) follows a similar goal, but uses a second revolute joint instead of a prismatic one. The Hoeckens linkage ABCDE generates the target ovoid curve at point E, which is then amplified by the pantograph EFGHIJ to produce the desired leg motion at

*Address all correspondence to this author.

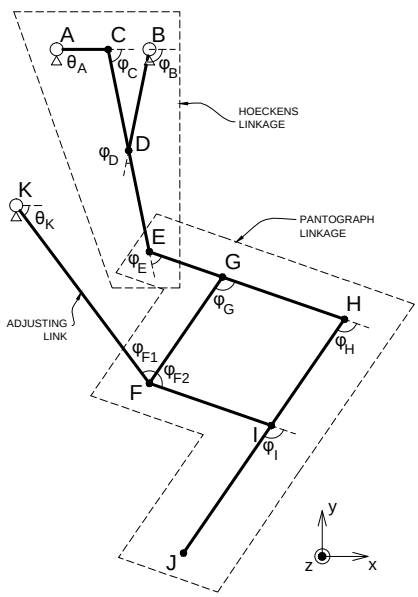


**FIGURE 1**. PROPOSED MECHANISM.

point J. The innovation lies in the adjusting link KF, which is used to change the position of the pantograph's pivot F. While a similar principle has previously been used in a prototype [10], the present work aims specifically to determine the kinematic equations of this mechanism and optimize its workspace using planar screw theory.

## KINEMATIC ANALYSIS

In order to determine the allowed displacements and the velocities of the mechanism's end-effector (namely the HJ link) screw theory [11] has been applied to each of the constituent linkages. Since the mechanism is planar, the two-dimensional expressions are used for the twists and wrenches [12]. Only the translations in the plane of motion ($\boldsymbol{\xi}_\infty$) and the rotations perpendicular to it ($\boldsymbol{\xi}_0$) are considered for the twists. Similarly, only the in-plane forces ($\boldsymbol{\zeta}_0$) and the out-of-plane torques ($\boldsymbol{\zeta}_\infty$) are considered for the wrenches.

### Mobility

The Hoeckens linkage, involving the A, B, C, D, and E joints, is a four-bar linkage, which can be decomposed in two parallel RR kinematic chains, AC and BD (cf. Fig. 2). The allowed displacements and the reciprocal wrenches of each chain, as well as the resulting screws for the coupler CE, are presented in Table 1. Vector $\mathbf{z}_X$ is the unit vector along the z-axis passing through point X. Vectors **mn** and similar are the unit vectors along the direction from point M to point N. The allowed displacements of CE, $V^{CE}$, are equivalent to the intersection of $V^1$ and $V^2$ and depend on the geometric configuration of the links. In the most general case the links AC and BD are not parallel. The corresponding mobility, $V_1^{CE}$, is a rotation of the coupler around the center $O_{CE}$, located at the intersection of AC and BD. In the initial position illustrated in Fig. 1, this point is superposed with B. During a full revolution of the crank AC, two particular configurations where the latter is parallel to the rocker BD change the instantaneous motion of the coupler to a translation perpendicular to AC and BD. This situation corresponds to the mobility $V_2^{CE}$. Finally, in a third case where AC and BD are collinear, the mobility $V_3^{CE}$ combines the two previous movements. If the allowed rotation is not infinitesimal (i.e. point C is superposed to point B and the coupler can freely rotate around it), the system is in a singularity. Such a configuration isn't advisable and must be avoided with an appropriate choice of lengths for each of the links.

The influence of each of the degrees of freedom ($\theta_A$ and $\theta_K$) on the movement of the leg (link HJ) will be analyzed independently. Thus, to understand the effect of a rotation of the crank

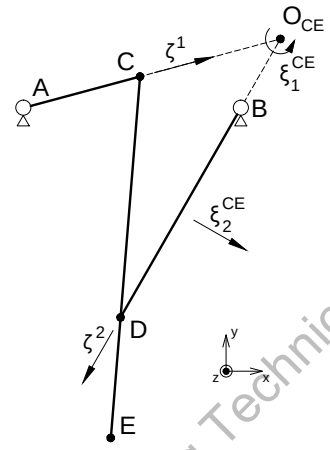


**FIGURE 2**. SCREWS FOR THE HOECKENS LINKAGE.

**TABLE 1**. SCREW SYSTEMS FOR THE HOECKENS LINKAGE.

| Chain | Screw system | Reciprocal screw system |
|---|---|---|
| AC | $V^1 = \{\boldsymbol{\xi}_0(\mathbf{z}_A), \boldsymbol{\xi}_0(\mathbf{z}_C)\}$ | $T^1 = \boldsymbol{\zeta}^1 = \{\boldsymbol{\zeta}_0(\mathbf{ac})\}$ |
| BD | $V^2 = \{\boldsymbol{\xi}_0(\mathbf{z}_B), \boldsymbol{\xi}_0(\mathbf{z}_D)\}$ | $T^2 = \boldsymbol{\zeta}^2 = \{\boldsymbol{\zeta}_0(\mathbf{bd})\}$ |
| | | $V_1^{CE} = \boldsymbol{\xi}_1^{CE} = \boldsymbol{\xi}_0(\mathbf{z}_{O_{CE}})$ |
| CE | $T^1 \bigcup T^2 = \{\boldsymbol{\zeta}_0(\mathbf{ac}), \boldsymbol{\zeta}_0(\mathbf{bd})\}$ | $V_2^{CE} = \boldsymbol{\xi}_2^{CE} = \boldsymbol{\xi}_\infty(\mathbf{ac} \times \mathbf{z})$ |
| | | $V_3^{CE} = \{\boldsymbol{\xi}_\infty(\mathbf{ac} \times \mathbf{z}), \boldsymbol{\xi}_0(\mathbf{z}_C)\}$ |

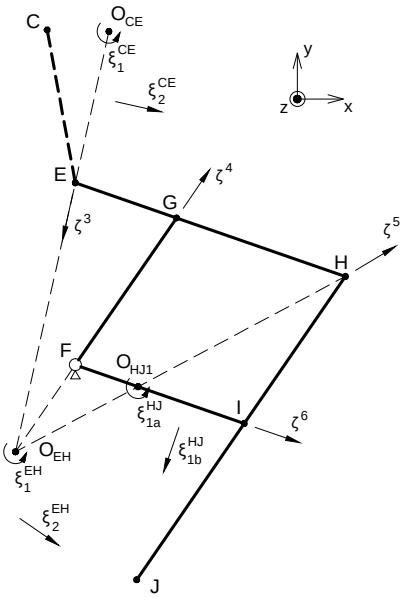


**FIGURE 3**. SCREWS FOR THE PANTOGRAPH (DOF 1).

**TABLE 2**. SCREW SYSTEMS FOR THE PANTOGRAPH (DOF 1).

| Chain | Screw system | Reciprocal screw system |
|---|---|---|
| E | $V^3 = \{\boldsymbol{\xi}_1^{CE} \text{ or } \boldsymbol{\xi}_2^{CE}, \boldsymbol{\xi}_0(\mathbf{z}_E)\}$ | $T^3 = \boldsymbol{\zeta}^3 = \{\boldsymbol{\zeta}_0(\mathbf{o}_{CE}\mathbf{e})\}$ |
| FG | $V^4 = \{\boldsymbol{\xi}_0(\mathbf{z}_F), \boldsymbol{\xi}_0(\mathbf{z}_G)\}$ | $T^4 = \boldsymbol{\zeta}^4 = \{\boldsymbol{\zeta}_0(\mathbf{fg})\}$ |
| EGH | $T^3 \bigcup T^4 = \{\boldsymbol{\zeta}_0(\mathbf{o}_{CE}\mathbf{e}), \boldsymbol{\zeta}_0(\mathbf{fg})\}$ | $V_1^{EH} = \boldsymbol{\xi}_1^{EH} = \boldsymbol{\xi}_0(\mathbf{z}_{O_{EH}})$<br>$V_2^{EH} = \boldsymbol{\xi}_2^{EH} = \boldsymbol{\xi}_\infty(\mathbf{fg} \times \mathbf{z})$<br>$V_3^{EH} = \{\boldsymbol{\xi}_\infty(\mathbf{fg} \times \mathbf{z}), \boldsymbol{\xi}_0(\mathbf{z}_E)\}$ |
| EH | $V^5 = \{\boldsymbol{\xi}_1^{EH} \text{ or } \boldsymbol{\xi}_2^{EH}, \boldsymbol{\xi}_0(\mathbf{z}_E)\}$ | $T^5 = \boldsymbol{\zeta}^5 = \{\boldsymbol{\zeta}_0(\mathbf{o}_{EH}\mathbf{h})\}$ |
| FI | $V^6 = \{\boldsymbol{\xi}_0(\mathbf{z}_F), \boldsymbol{\xi}_0(\mathbf{z}_I)\}$ | $T^6 = \boldsymbol{\zeta}^6 = \{\boldsymbol{\zeta}_0(\mathbf{fi})\}$ |
| HIJ | $T^5 \bigcup T^6 = \{\boldsymbol{\zeta}_0(\mathbf{o}_{EH}\mathbf{h}), \boldsymbol{\zeta}_0(\mathbf{fi})\}$ | $V_{1a}^{HJ} = \boldsymbol{\xi}_{1a}^{EH} = \boldsymbol{\xi}_0(\mathbf{z}_{O_{HJ1}})$<br>$V_{1b}^{HJ} = \boldsymbol{\xi}_2^{HJ} = \boldsymbol{\xi}_\infty(\mathbf{fi} \times \mathbf{z})$<br>$V_{1c}^{HJ} = \{\boldsymbol{\xi}_\infty(\mathbf{fi} \times \mathbf{z}), \boldsymbol{\xi}_0(\mathbf{z}_E)\}$ |

AC, the KF link is first considered as static, which is equivalent to place a fixed pivot joint at point F (cf. Fig. 3). The Hoeckens linkage is then only modeled by its effect, namely the rotation of CE around $O_{CE}$ (or a translation in a configuration where $V_2^{CE}$ is valid). The sequential resolution of the mobility of the pantograph linkage is presented in Table 2. First, two serial chains, CE and FG are used to find the allowed displacements of the link EH. It appears quickly that the nature of the displacement of CE

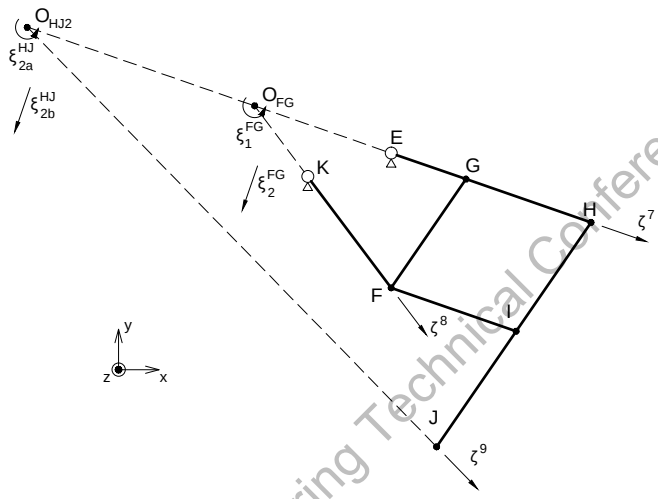


**FIGURE 4**. SCREWS FOR THE PANTOGRAPH (DOF 2).

(rotation $xi_1^{CE}$ or translation $xi_2^{CE}$) does not affect the nature of the displacement of EH. The reciprocal screw, in both cases, corresponds to a force, which is either directed from $O_{CE}$ to E or parallel to AC. Three possibilities again exist for the movement of EH: a rotation ($V_1^{EH}$), a translation ($V_1^{EH}$), or a combination of both ($V_3^{EH}$). The third mobility is only possible if EG and FG are collinear, a geometric configuration equivalent to a degenerate parallelogram, which is a singularity of the mechanism.

Once the allowed rotation or translation of the link EH is identified, a similar analysis is repeated for the terminal link HJ. For a non-degenerate parallelogram, the allowed displacement is either a rotation relative to a center $O_{HJ1}$, located on the line FI (in the initial configuration, this center is superposed with F) or a translation perpendicular to FI. The geometric configurations which generate a translation are either that the projected intersection of AC and BD is on the line EH, or that AC, BD, FG, and HJ are all parallel and perpendicular to EH and FI.

An identical approach is used to determine the influence of the adjusting link (rotation of $\theta_K$) on the terminal link HJ, this time by placing a fixed pivot joint at the point E (cf. Fig. 4). Again, two possibilities of movement exist for a non-degenerate parallelogram as presented in Table 3. This mobility is transmitted to the link HJ by the pantograph. The following relationship can be used to locate the center of rotation of HJ for the second degree of freedom:

$$\frac{\mathbf{eo}_{HJ2}}{\mathbf{eo}_{FG}} = \frac{\mathbf{eh}}{\mathbf{eg}} \tag{1}$$

**TABLE 3**. SCREW SYSTEMS FOR THE PANTOGRAPH (DOF 2).

| Chain | Twist system | Reciprocal wrench system |
|---|---|---|
| EG | $V^7 = \{\boldsymbol{\xi}_0(\mathbf{z}_E), \boldsymbol{\xi}_0(\mathbf{z}_G)\}$ | $T^7 = \boldsymbol{\zeta}^7 = \{\boldsymbol{\zeta}_0(\mathbf{eg})\}$ |
| KF | $V^8 = \{\boldsymbol{\xi}_0(\mathbf{z}_K), \boldsymbol{\xi}_0(\mathbf{z}_F)\}$ | $T^8 = \boldsymbol{\zeta}^8 = \{\boldsymbol{\zeta}_0(\mathbf{kf})\}$ |
| | | $V_1^{FG} = \boldsymbol{\xi}_1^{FG} = \boldsymbol{\xi}_0(\mathbf{z}_{O_{FG}})$ |
| FG | $T^7 \bigcup T^8 = \{\boldsymbol{\zeta}_0(\mathbf{eg}), \boldsymbol{\zeta}_0(\mathbf{kf})\}$ | $V_2^{FG} = \boldsymbol{\xi}_2^{FG} = \boldsymbol{\xi}_\infty(\mathbf{kf} \times \mathbf{z})$ |
| | | $V_3^{FG} = \{\boldsymbol{\xi}_\infty(\mathbf{kf} \times \mathbf{z}), \boldsymbol{\xi}_0(\mathbf{z}_H)\}$ |

## Equations of movement

It is now possible to determine the quantitative relationships between the input and output variables, respectively the angular velocities $\dot{\theta}_A$ and $\dot{\theta}_K$ and the velocities of the terminal link. First, the twist of the coupler of the Hoeckens linkage, $\boldsymbol{\xi}^{CE}$, is defined, with $\dot{\phi}_i$ the passive velocity magnitude associated with joint i:

$$\boldsymbol{\xi}^{CE} = \dot{\theta}_A \boldsymbol{\xi}_0(\mathbf{z}_A) + \dot{\phi}_C \boldsymbol{\xi}_0(\mathbf{z}_C) = \dot{\phi}_B \boldsymbol{\xi}_0(\mathbf{z}_B) + \dot{\phi}_D \boldsymbol{\xi}_0(\mathbf{z}_D) \tag{2}$$

The passive rotations can be eliminated from this equation by using the reciprocal product with carefully chosen reciprocal wrenches, i.e.:

$$\boldsymbol{\xi}^{CE} \circ \boldsymbol{\zeta}_0(\mathbf{x}_C) = \dot{\theta}_A \boldsymbol{\xi}_0(\mathbf{z}_A) \circ \boldsymbol{\zeta}_0(\mathbf{x}_C) \tag{3a}$$
$$\boldsymbol{\xi}^{CE} \circ \boldsymbol{\zeta}_0(\mathbf{y}_C) = \dot{\theta}_A \boldsymbol{\xi}_0(\mathbf{z}_A) \circ \boldsymbol{\zeta}_0(\mathbf{y}_C) \tag{3b}$$
$$\boldsymbol{\xi}^{CE} \circ \boldsymbol{\zeta}_0(\mathbf{bd}) = 0 \tag{3c}$$

With the following definition for the previous screws, where P is the point for which the velocities are computed:

$$\boldsymbol{\xi}_0(\mathbf{z}_A) = \begin{bmatrix} \mathbf{z} \\ \mathbf{z} \times \mathbf{ap} \end{bmatrix} = \begin{bmatrix} 1 \\ \mathbf{ap}^T\mathbf{y} \\ \mathbf{ap}^T\mathbf{x} \end{bmatrix} \tag{4a}$$
$$\boldsymbol{\xi}_0(\mathbf{x}_C) = \begin{bmatrix} \mathbf{x} \\ \mathbf{x} \times \mathbf{cp} \end{bmatrix} = \begin{bmatrix} 1 \\ 0 \\ \mathbf{cp}^T\mathbf{y} \end{bmatrix} \tag{4b}$$
$$\boldsymbol{\xi}_0(\mathbf{bd}) = \begin{bmatrix} \mathbf{bd} \\ \mathbf{bd} \times \mathbf{bp} \end{bmatrix} = \begin{bmatrix} \mathbf{bd}^T\mathbf{x} \\ \mathbf{bd}^T\mathbf{y} \\ (\mathbf{bd} \times \mathbf{bp})^T\mathbf{z} \end{bmatrix} \tag{4c}$$

It would also have been possible to choose the screws in order to have an equivalent equation system with two of the right-hand terms being zero:

$$\boldsymbol{\xi}^{CE} \circ \boldsymbol{\zeta}_0(\mathbf{ac} \times \mathbf{z}) = \dot{\theta}_A \boldsymbol{\xi}_0(\mathbf{z}_A) \circ \boldsymbol{\zeta}_0(\mathbf{ac} \times \mathbf{z}) \tag{5a}$$
$$\boldsymbol{\xi}^{CE} \circ \boldsymbol{\zeta}_0(\mathbf{ac}) = 0 \tag{5b}$$
$$\boldsymbol{\xi}^{CE} \circ \boldsymbol{\zeta}_0(\mathbf{bd}) = 0 \tag{5c}$$

However, a choice was rather made to simplify the expression of the left-hand terms. In matrix form, the equations of movement of the Hoeckens linkage are then:

$$\mathbf{A}\boldsymbol{\xi}^{CE} = \mathbf{b}\dot{\theta}_A \tag{6a}$$
$$\begin{bmatrix} \boldsymbol{\zeta}_0(\mathbf{x}_C)\circ \\ \boldsymbol{\zeta}_0(\mathbf{y}_C)\circ \\ \boldsymbol{\zeta}_0(\mathbf{bd})\circ \end{bmatrix} \boldsymbol{\xi}^{CE} = \begin{bmatrix} \boldsymbol{\xi}_0(\mathbf{z}_A) \circ \boldsymbol{\zeta}_0(\mathbf{x}_C) \\ \boldsymbol{\xi}_0(\mathbf{z}_A) \circ \boldsymbol{\zeta}_0(\mathbf{y}_C) \\ 0 \end{bmatrix} \dot{\theta}_A \tag{6b}$$

The following simplifications can also be made:

$$\boldsymbol{\xi}_0(\mathbf{z}_A) \circ \boldsymbol{\zeta}_0(\mathbf{x}_C) = \mathbf{cp}^T\mathbf{y} - \mathbf{ap}^T\mathbf{y} = -\mathbf{ac}^T\mathbf{y} \tag{7a}$$
$$\boldsymbol{\xi}_0(\mathbf{z}_A) \circ \boldsymbol{\zeta}_0(\mathbf{y}_C) = \mathbf{ap}^T\mathbf{x} - \mathbf{cp}^T\mathbf{x} = \mathbf{ac}^T\mathbf{x} \tag{7b}$$

Thus, the Jacobian matrices A and b of the Hoeckens linkage can be written as:

$$\begin{bmatrix} \mathbf{cp}^T\mathbf{y} & 1 & 0 \\ -\mathbf{cp}^T\mathbf{x} & 0 & 1 \\ (\mathbf{bd} \times \mathbf{bp})^T\mathbf{z} & \mathbf{bd}^T\mathbf{x} & \mathbf{bd}^T\mathbf{y} \end{bmatrix} \boldsymbol{\xi}^{CE} = \begin{bmatrix} -\mathbf{ac}^T\mathbf{y} \\ \mathbf{ac}^T\mathbf{x} \\ 0 \end{bmatrix} \dot{\theta}_A \tag{8a}$$
$$\boldsymbol{\xi}^{CE} = \mathbf{A}^{-1}\mathbf{b}\dot{\theta}_A \tag{8b}$$

Next, the twist of the link EH is expressed as a combination of $\boldsymbol{\xi}^{CE}$ and $\dot{\theta}_A$:

$$\boldsymbol{\xi}^{EH} = \boldsymbol{\xi}^{CE} + \dot{\phi}_E \boldsymbol{\xi}_0(\mathbf{z}_E) = \mathbf{A}^{-1}\mathbf{b}\dot{\theta}_A + \dot{\phi}_E \boldsymbol{\xi}_0(\mathbf{z}_E) \tag{9a}$$
$$\boldsymbol{\xi}^{EH} = \dot{\theta}_K \boldsymbol{\xi}_0(\mathbf{z}_K) + \dot{\phi}_{F1} \boldsymbol{\xi}_0(\mathbf{z}_F) + \dot{\phi}_G \boldsymbol{\xi}_0(\mathbf{z}_G) \tag{9b}$$

And the passive velocities are eliminated:

$$\boldsymbol{\xi}^{EH} \circ \boldsymbol{\zeta}_0(\mathbf{x}_E) = \dot{\theta}_A \mathbf{A}^{-1}\mathbf{b} \circ \boldsymbol{\zeta}_0(\mathbf{x}_E) \tag{10a}$$
$$\boldsymbol{\xi}^{EH} \circ \boldsymbol{\zeta}_0(\mathbf{y}_E) = \dot{\theta}_A \mathbf{A}^{-1}\mathbf{b} \circ \boldsymbol{\zeta}_0(\mathbf{y}_E) \tag{10b}$$
$$\boldsymbol{\xi}^{EH} \circ \boldsymbol{\zeta}_0(\mathbf{fg}) = \dot{\theta}_K \boldsymbol{\xi}_0(\mathbf{z}_K) \circ \boldsymbol{\zeta}_0(\mathbf{fg}) \tag{10c}$$

With the following simplification:

$$\dot{\theta}_K \boldsymbol{\xi}_0(\mathbf{z}_K) \circ \boldsymbol{\zeta}_0(\mathbf{fg}) = (\mathbf{fg} \times \mathbf{fp})^T\mathbf{z} - (\mathbf{fg} \times \mathbf{kp})^T\mathbf{z} \tag{11a}$$
$$\dot{\theta}_K \boldsymbol{\xi}_0(\mathbf{z}_K) \circ \boldsymbol{\zeta}_0(\mathbf{fg}) = (\mathbf{fg} \times (\mathbf{fp} - \mathbf{kp}))^T\mathbf{z} \tag{11b}$$
$$\dot{\theta}_K \boldsymbol{\xi}_0(\mathbf{z}_K) \circ \boldsymbol{\zeta}_0(\mathbf{fg}) = (\mathbf{kf} \times \mathbf{fg})^T\mathbf{z} \tag{11c}$$

In matrix form, one has:

$$\mathbf{C}\boldsymbol{\xi}^{EH} = \mathbf{D}\begin{bmatrix}\dot{\theta}_A\\ \dot{\theta}_K\end{bmatrix} \quad (12a)$$

$$\begin{bmatrix}\boldsymbol{\zeta}_0(\mathbf{x}_E)\circ\\ \boldsymbol{\zeta}_0(\mathbf{y}_E)\circ\\ \boldsymbol{\zeta}_0(\mathbf{fg})\circ\end{bmatrix}\boldsymbol{\xi}^{EH} = \begin{bmatrix}\mathbf{A}^{-1}\mathbf{b}\circ\boldsymbol{\zeta}_0(\mathbf{x}_E) & 0\\ \mathbf{A}^{-1}\mathbf{b}\circ\boldsymbol{\zeta}_0(\mathbf{y}_E) & 0\\ 0 & (\mathbf{kf}\times\mathbf{fg})^T\mathbf{z}\end{bmatrix}\begin{bmatrix}\dot{\theta}_A\\ \dot{\theta}_K\end{bmatrix} \quad (12b)$$

The Jacobian matrices **C** and **D** of the link EH are then:

$$\mathbf{C} = \begin{bmatrix}\mathbf{ep}^T\mathbf{y} & 1 & 0\\ -\mathbf{ep}^T\mathbf{x} & 0 & 1\\ (\mathbf{fg}\times\mathbf{fp})^T\mathbf{z} & \mathbf{fg}^T\mathbf{x} & \mathbf{fg}^T\mathbf{y}\end{bmatrix} \quad (13a)$$

$$\mathbf{D} = \begin{bmatrix}\mathbf{A}^{-1}\mathbf{b}\circ\boldsymbol{\zeta}_0(\mathbf{x}_E) & 0\\ \mathbf{A}^{-1}\mathbf{b}\circ\boldsymbol{\zeta}_0(\mathbf{y}_E) & 0\\ 0 & (\mathbf{kf}\times\mathbf{fg})^T\mathbf{z}\end{bmatrix} \quad (13b)$$

The following formulation, where $(\mathbf{C}^{-1}\mathbf{D})_i$ is the i-th column of $\mathbf{C}^{-1}\mathbf{D}$, can also be used:

$$\boldsymbol{\xi}^{EH} = \mathbf{C}^{-1}\mathbf{D}\begin{bmatrix}\dot{\theta}_A\\ \dot{\theta}_K\end{bmatrix} = (\mathbf{C}^{-1}\mathbf{D})_1\dot{\theta}_A + (\mathbf{C}^{-1}\mathbf{D})_2\dot{\theta}_K \quad (14)$$

The same method is finally applied to the terminal link of the mechanism:

$$\boldsymbol{\xi}^{HJ} = (\mathbf{C}^{-1}\mathbf{D})_1\dot{\theta}_A + (\mathbf{C}^{-1}\mathbf{D})_2\dot{\theta}_K + \dot{\phi}_H\boldsymbol{\xi}_0(\mathbf{z}_H) \quad (15a)$$

$$\boldsymbol{\xi}^{HJ} = \dot{\theta}_K\boldsymbol{\xi}_0(\mathbf{z}_K) + (\dot{\phi}_{F1}+\dot{\phi}_{F2})\boldsymbol{\xi}_0(\mathbf{z}_F) + \dot{\phi}_I\boldsymbol{\xi}_0(\mathbf{z}_I) \quad (15b)$$

$$\boldsymbol{\xi}^{HJ}\circ\boldsymbol{\zeta}_0(\mathbf{x}_H) = (\dot{\theta}_A(\mathbf{C}^{-1}\mathbf{D})_1 + \dot{\theta}_K(\mathbf{C}^{-1}\mathbf{D})_2)\circ\boldsymbol{\zeta}_0(\mathbf{x}_H) \quad (15c)$$

$$\boldsymbol{\xi}^{HJ}\circ\boldsymbol{\zeta}_0(\mathbf{y}_H) = (\dot{\theta}_A(\mathbf{C}^{-1}\mathbf{D})_1 + \dot{\theta}_K(\mathbf{C}^{-1}\mathbf{D})_2)\circ\boldsymbol{\zeta}_0(\mathbf{y}_H) \quad (15d)$$

$$\boldsymbol{\xi}^{HJ}\circ\boldsymbol{\zeta}_0(\mathbf{fi}) = \dot{\theta}_K\boldsymbol{\xi}_0(\mathbf{z}_K)\circ\boldsymbol{\zeta}_0(\mathbf{fi}) \quad (15e)$$

In matrix form, with similar simplifications as the previous stage, one obtains:

$$\mathbf{E}\boldsymbol{\xi}^{HJ} = \mathbf{F}\begin{bmatrix}\dot{\theta}_A\\ \dot{\theta}_K\end{bmatrix} \quad (16a)$$

$$\mathbf{E} = \begin{bmatrix}\mathbf{hp}^T\mathbf{y} & 1 & 0\\ -\mathbf{hp}^T\mathbf{x} & 0 & 1\\ (\mathbf{fi}\times\mathbf{fp})^T\mathbf{z} & \mathbf{fi}^T\mathbf{x} & \mathbf{fi}^T\mathbf{y}\end{bmatrix} \quad (16b)$$

$$\mathbf{F} = \begin{bmatrix}(\mathbf{C}^{-1}\mathbf{D})_1\circ\boldsymbol{\zeta}_0(\mathbf{x}_H) & (\mathbf{C}^{-1}\mathbf{D})_2\circ\boldsymbol{\zeta}_0(\mathbf{x}_H)\\ (\mathbf{C}^{-1}\mathbf{D})_1\circ\boldsymbol{\zeta}_0(\mathbf{y}_H) & (\mathbf{C}^{-1}\mathbf{D})_2\circ\boldsymbol{\zeta}_0(\mathbf{y}_H)\\ 0 & (\mathbf{kf}\times\mathbf{fi})^T\mathbf{z}\end{bmatrix} \quad (16c)$$

$$\boldsymbol{\xi}^{HI} = \mathbf{E}^{-1}\mathbf{F}\begin{bmatrix}\dot{\theta}_A\\ \dot{\theta}_K\end{bmatrix} \quad (16d)$$

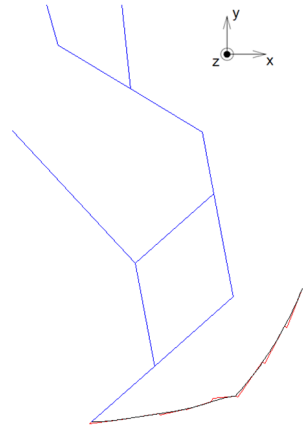


**FIGURE 5**. VALIDATION OF THE KINEMATIC RELATIONSHIPS.

To estimate the velocities at the extremity of the link HJ, the coordinates of the point P in matrices **A** to **F** must correspond to these of point J. Likewise, it is easy to consider a robotic feet of arbitrary dimensions attached to the end of the leg by choosing the appropriate coordinates for the point P for which the velocities are computed.

## Validation

The Jacobian matrices of the system have been numerically validated along an arbitrary trajectory involving a rotation of both degrees of freedom. Fig. 5 shows a discretization of the trajectory, in black, as well as an extrapolation of the trajectory based on the velocities at each point, in red. As expected, the red curve follows very closely the black one, especially when its curvature is relatively low. These results confirm numerically the calculated Jacobian matrices.

## Singularities

The existence of a solution to the equation $\boldsymbol{\xi}^{HI} = \mathbf{E}^{-1}\mathbf{F}\dot{\boldsymbol{\theta}}$ (with $\dot{\boldsymbol{\theta}} = [\dot{\theta}_A\,\dot{\theta}_K]^T$) is conditional to each of the matrices $\boldsymbol{A}$, $\boldsymbol{C}$ and $\boldsymbol{E}$ being non-singular. The determinants of these matrices can be evaluated as follows:

$$\det(\mathbf{A}) = \det\begin{bmatrix}\mathbf{cp}^T\mathbf{y} & 1 & 0\\ -\mathbf{cp}^T\mathbf{x} & 0 & 1\\ (\mathbf{bd}\times\mathbf{bp})^T\mathbf{z} & \mathbf{bd}^T\mathbf{x} & \mathbf{bd}^T\mathbf{y}\end{bmatrix} \quad (17a)$$

$$= (\mathbf{bd}\times\mathbf{bp})^T\mathbf{z} - (\mathbf{bd}^T\mathbf{x})(\mathbf{cp}^T\mathbf{y}) + (\mathbf{bd}^T\mathbf{y})(\mathbf{cp}^T\mathbf{x}) \quad (17b)$$

$$= (\mathbf{bd}\times\mathbf{bp})^T\mathbf{z} - (\mathbf{bd}\times\mathbf{cp})^T\mathbf{z} \quad (17c)$$

$$= (\mathbf{bd}\times(\mathbf{bp}-\mathbf{cp}))^T\mathbf{z} \quad (17d)$$

$$\det(\mathbf{A}) = (\mathbf{bd}\times\mathbf{bc})^T\mathbf{z} \quad (17e)$$

**TABLE 4**. SINGULARITIES OF THE MECHANISM.

| | | |
|---|---|---|
| | Hoeckens linkage | |
| Type 1 | $\lvert\mathbf{ac}\rvert = 0$ | Loss of the first DOF |
| | ABCD Aligned | Degenerate 4-bar: Infinitesimal mobility gain |
| | BC Superposed | Degenerate 4-bar: Complete mobility gain (Fig. 6II) |
| Type 2 | $\lvert\mathbf{cd}\rvert = \mathbf{0}$ | Mobility gain |
| | $\lvert\mathbf{bd}\rvert = \mathbf{0}$ | Mobility loss |
| | $\lvert\mathbf{cd}\rvert + \lvert\mathbf{bd}\rvert < \lvert\mathbf{bd}\rvert + \lvert\mathbf{bd}\rvert$ | Grashof condition: Mobility loss (Fig. 6III) |
| | Adjusting link and pantograph | |
| Type 1 | $\lvert\mathbf{kf}\rvert = 0$ | Loss of the second DOF |
| | FGHI Aligned | Degenerate parallelogram: Mobility loss (Fig. 6I) |
| | FH Superposed | Degenerate parallelogram: Complete mobility gain |
| Type 2 | $\lvert\mathbf{fg}\rvert = \mathbf{0}$ | Mobility loss |
| | $\lvert\mathbf{eg}\rvert = \mathbf{0}$ | Mobility gain |
| | $\lvert\mathbf{fi}\rvert = \mathbf{0}$ | Mobility loss |
| | $\lvert\mathbf{hi}\rvert = \mathbf{0}$ | Mobility gain |

Similarly, for the other matrices, one obtains:

$$\det(\mathbf{C}) = (\mathbf{fg} \times \mathbf{fe})^T \mathbf{z} \tag{18a}$$

$$\det(\mathbf{E}) = (\mathbf{fi} \times \mathbf{fh})^T \mathbf{z} \tag{18b}$$

Some of the singularities have already been exposed during the mobility analysis. The latter along all of the other possible cases are presented in Table 4. Most of these cases are purely theoretical, since a length of 0 for any link would obviously compromise the correct functionality of the mechanism. The Hoeckens linkage singularities, shown in Figs. 6II and 6III can be avoided by carefully imposing the limits for the lengths of each link: $\lvert\mathbf{ac}\rvert \neq \lvert\mathbf{ab}\rvert$ and $\lvert\mathbf{cd}\rvert + \lvert\mathbf{db}\rvert > \lvert\mathbf{ac}\rvert + \lvert\mathbf{ab}\rvert$ (Grashof condition). A degenerescence of the pantograph (Fig. 6I) is harder to avoid, and happens when the angle $\phi_G$ is equal to 0.

## Workspace

There often exists a direct link between the singularities of a mechanism and the limits of its workspace. In the present case, the workspace corresponds to all the positions which can be reached by the leg's extremity (point J), and is represented by

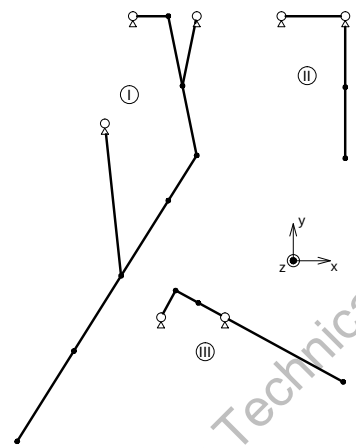


**FIGURE 6**. SOME SINGULAR CONFIGURATIONS.

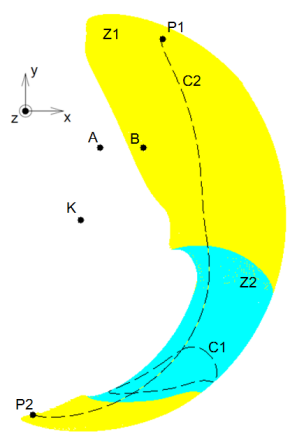


**FIGURE 7**. WORKSPACE OF THE MECHANISM.

the yellow area $Z_1$ in Fig. 7. This zone has been drawn by considering all possible combinations $[0, 2\pi]$ for the input variables of the mechanism ($\theta_A$ and $\theta_K$). Note the position of the fixed pivots A, B, and K in this figure. However, a more interesting subset of the global workspace named $Z_2$ holds all the points for which a complete rotation of the crank is possible without encountering a singular configuration. This zone is limited by the degenerate pantograph singularities. By considering a constant orientation for the adjusting link ($\theta_K$) and by turning solely the crank's angle ($\theta_A$), the curve $C_1$ is obtained. Similarly, the curve $C_2$ is drawn for the second degree of freedom. The points $P_1$ and $P_2$ limit the possible values of $\theta_K$ for the chosen $\theta_A$ and correspond also to degenerate pantograph singularities. More extreme values of $\theta_K$ can be reached for different crank angles, and establish the true superior and inferior limits of $Z_1$.

## Static Analysis

The Jacobian matrices previously identified are also useful for the study of the forces present in the mechanism [13]. A dynamic analysis taking in consideration the mass of the robot, the accelerations, and the position of the point of contact with the ground P can provide the required forces $F_{px}$ and $F_{py}$ that the foot must apply to the ground. Neglecting the dynamics of the leg itself, the driving torques $\tau_A$ and $\tau_K$ can be deduced by the following quasi-static relationship:

$$\boldsymbol{\tau} = \mathbf{J}^T\mathbf{f} \qquad \begin{bmatrix}\tau_A\\ \tau_K\end{bmatrix} = (\mathbf{E}^{-1}\mathbf{F})^T \begin{bmatrix}\tau_P\\ F_{px}\\ F_{py}\end{bmatrix} \tag{19}$$

This equation was validated by solving numerically the 24 static equilibrium equations of the mechanism and comparing this result with the above relationship.

## OPTIMIZATION

In order to optimize the performances of the mechanism, a genetic algorithm has been used to choose the best lengths for the links, and the best positions for the fixed pivots A, B and K. For each individual, the algorithm evaluates the shape of the zone $Z_2$, the subset of the workspace for which a full rotation of the crank is possible. To evaluate the quality of the result, an objective function inspired by the literature is used [14], namely:

$$f = \frac{1}{I_{stride} I_{clearance}} \tag{20a}$$

$$\text{where} \quad I_{stride} = \frac{max(x) - min(x)}{L} \tag{20b}$$

$$\text{and} \quad I_{clearance} = \frac{max(y) - min(y)}{L} \tag{20c}$$

The coordinates x and y are the position of each point forming $Z_2$. A normalization of the performance indexes for the stride and the clearance is realized by dividing them by the conventional length of the leg $|\mathbf{bd}| + |\mathbf{de}| + |\mathbf{eh}| + |\mathbf{hi}|$, in order to prevent purely an increase in size of the mechanism. Table 5 presents the dimensions and the performance index of the best individual found illustrated in Fig. 8, comparatively to the initial configuration presented in this article. Please note that the frame of the figure is slightly tilted to emphasize the possible alignment of the straight part of the trajectory with the horizontal axis of the page. For Table 5, the values in italics are fixed parameters.

## DISCUSSION

The use of mechanical deformations to produce the desired motion, or compliance, is an interesting alternative to the use of mechanical joints in a mechanism. First, the ranges of motion for each joint of the optimized mechanism are evaluated for two different paths of the foot (Table 6). The path $C_1$ (Fig. 8) is obtained by using only the first degree of freedom ($\theta_A$), whereas $C_3$ (Fig. 8) is a possible use of the adjusting link to increase step height. It is evident that at least two joints, A and C, have to remain fully rotative to keep the mobility of the mechanism.

**TABLE 5**. CARACTERISTICS OF THE OPTIMIZED DESIGN.

| Parameter | Initial configuration | Optimized configuration |
|---|---|---|
| Point A | *(0,0)* | *(0,0)* |
| Point B | (1.8, *0*) | (3.4, *0*) |
| Point K | (-0.8,3) | (-0.3,-1.2) |
| $\|\mathbf{ac}\|$ | *1* | *1* |
| $\|\mathbf{cd}\|$ | 2 | 2.7 |
| $\|\mathbf{bd}\|$ | 2 | 3.1 |
| $\|\mathbf{de}\|$ | 2 | 0.5 |
| $\|\mathbf{eg}\|$ | 1.5 | 1.8 |
| $\|\mathbf{gh}\| = \|\mathbf{fi}\|$ | 2.5 | 4.1 |
| $\|\mathbf{fg}\| = \|\mathbf{hi}\|$ | 2.5 | 2.6 |
| $\|\mathbf{ij}\|$ | 2 | 4.1 |
| $\|\mathbf{fk}\|$ | 4.3 | 4.8 |
| $I_{stride}$ | 0.62 | 1.13 |
| $I_{clearance}$ | 0.52 | 1.32 |
| $f$ | 3.05 | 0.67 |

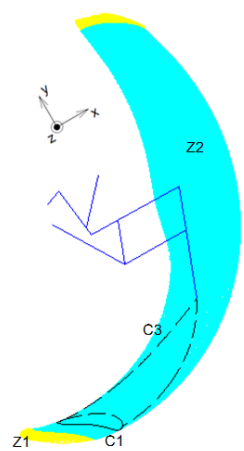


**FIGURE 8**. WORKSPACE AFTER OPTIMIZATION, ROTATED.

**TABLE 6**. ROTATION RANGES OF THE JOINTS.

| Joint | $C_1$ | $C_3$ |
|---|---|---|
| $\theta_A$ | 360° | 360° |
| $\theta_K$ | 0° | 34° |
| $\phi_B$ | 39° | 39° |
| $\phi_C$ | 360° | 360° |
| $\phi_D$ | 51° | 51° |
| $\phi_E$ | 89° | 92° |
| $\phi_{F1}$ | 29° | 51° |
| $\phi_{F2} = \phi_G = \phi_H = \phi_I$ | 52° | 115° |

**FIGURE 9**. 3D PRINTED PROTOTYPE.

Several goals can be pursued by designing a compliant mechanism. It is possible to use the mechanical deformation as a way to store energy during a fraction of the motion cycle and restore it later. Preventing rotation at joint B, for example, would be a way to add compliance to the rocker of the Hoeckens linkage and balance the torque requirements of the crank motor between the supporting and swinging phases of the leg [10]. Another promising option is to use compliance to provide damping to the mechanism. A 3D printed prototype of the optimized design has been built and is illustrated in Fig.9.

## CONCLUSIONS

In this paper, a common design for one-DOF robotic legs, the Hoeckens architecture, is augmented adding a second degree of freedom to control step height. The kinematic equations of the proposed mechanism are derived using screw theory. The main geometric constraint limiting the mobility of the robotic leg is a degenerescence of the pantograph at the limits of the workspace. Using a genetic algorithm for the selection of the geometric parameters of the mechanism, the size of the workspace has been greatly increased, promising improved obstacle overpassing capabilities compared to the original design.

## REFERENCES


[1] McKendry, J., Brown, B., Westervelt, E., and Schmiedeler, J., 2008. "Design and analysis of a class of planar biped robots mechanically coordinated by a single degree of freedom". *Journal of Mechanical Design,* ***130***(10), October, p. 102302.

[2] Funabashi, H., Ogawa, K., Gotoh, Y., and Kojima, F., 1985. "Synthesis of leg-mechanisms of biped walking machines part 1, synthesis of ankle-path-generator". *Bulletin of JSME,* ***28***(237), March, pp. 537–543.

[3] Shieh, W., Tsai, L.-W., and Azarm, S., 1997. "Design and optimization of a one-degree-of-freedom six-bar leg mechanism for a walking machine". *Journal of Robotic Systems,* ***14***(12), pp. 871–880.

[4] Chen, C., Chen, I., and Cheng, C., 2009. "Integrated design of legged mechatronic system". *Frontiers of Mechanical Engineering,* ***4***(3), pp. 264–275.

[5] Ottaviano, E., and Rea, P., 2013. "Design and operation of a 2-dof leg?wheel hybrid robot". *Robotica,* ***31***, pp. 1319–1325.

[6] Liang, C., Ceccarelli, M., and Takeda, Y., 2012. "Operation analysis of a chebyshev-pantograph leg mechanism for a single dof biped robot". *Frontiers of Mechanical Engineering,* ***7***(4), pp. 357–370.

[7] Liang, C., Ceccarelli, M., and Carbone, G., 2009. "A novel biologically inspired tripod walking robot". In Proceedings of the 13th WSEAS International Conference on SYSTEMS, N. Mastorakis, ed., World Scientific and Engineering Academy and Society, pp. 83–91.

[8] Ottaviano, E., Ceccarelli, M., and Tavolieri, C., 2004. "Kinematic and dynamic analyses of a pantograph-leg for a biped walking machine". In Proceedings of the 7th International Conference Climbing and Walking Robots, M. Armada and P. G. de Santos, eds., CLAWAR, Springer, pp. 561–568.

[9] Ceccarelli, M., Carbone, G., and Ottaviano, E., 2010. "Mechanism solutions for legged robots overcoming obstacles". In *New Trends in Mechanism Science*, D. Pisla, ed., Vol. 5 of *Mechanisms and machine science*. Springer, Berlin, pp. 545–553.

[10] Williams, R., Tsai, L., and Azarm, S., 1991. "Design of a crank-and-rocker driven pantograph: a leg mechanism for the university of maryland?s 1991 walking robot". In Proceedings of the 2nd National Conference on Applied Mechanisms and Robotics, Vol. 1. Paper number VI B.2.

[11] Ball, R., 1900. *A Treatise on the Theory of Screws*. Cambridge University Press, Cambridge, UK.
[12] Bonev, I., Zlatanov, D., and Gosselin, C., 2003. "Singularity analysis of 3-dof planar parallel mechanisms via screw theory". *Journal of Mechanical Design,* ***125***(3), September, pp. 573–581.
[13] Angeles, J., 2014. *Fundamentals of Robotic Mechanical Systems*. Springer, Switzerland.
[14] Birglen, L., and Ruella, C., 2014. "Analysis and optimization of one-degree of freedom robotic legs". *Mechanisms Robotics,* ***6***(4), November, p. 041004.